A discrete element method to model coating layer mechanical properties with bimodal and pseudo-full particle size distributions

DANIEL VARNEY, MARTTI TOIVAKKA, AND DOUGLAS W. BOUSFIELD

ABSTRACT: The mechanical properties of paper coating layers are important in converting operations such as calendering, printing, and folding. While several experimental and theoretical studies have advanced our knowledge of these systems, a particle level understanding of issues like crack-at-the-fold are lacking.

A discrete element method (DEM) model is used to describe bending and tension deformations of a coating layer. The particles in the model are either bimodal distributions or pseudo-full particle size distributions of spherical particles. The impact of particle size distribution on the predicted mechanical properties of the coating layer is reported. Inputs to the model include properties of the binder film and the binder concentration. The model predicts crack formation as a function of these parameters and also calculates the modulus, the maximum stress, and the strain-to-failure.

The simulation results are compared to previous experimental results. Reasonable predictions were obtained for both tensile and bending for a range of latex-starch ratios and at various binder concentrations. The influence of particle packing density on mechanical properties is reported.

Application: A model is proposed that helps predict the mechanical properties of a coating layer based on pigment size distribution and binder properties.

Mechanical properties of coatings are important in a number of applications. For coated papers, the resistance to picking during the printing operation is critical, as well as is the ability for the sample to be converted or folded without cracking of the coating layer [1,2]. The increased use of starch as a binder is of interest as the industry tries to move to natural binders, but starch often increases cracking problems [3,4].

The occurrence of cracks in barrier coatings is important to predict. If the coating layer is a homogenous material, such as a specific polymer, the mechanical properties of the layer can be estimated from the bulk properties of that material. However, when the coating layer is a porous composite of pigments and binder, the mechanical properties are more difficult to predict.

Finite element methods (FEM) can be used to simulate the deformation of coated paper by treating the coating layer as a continuum [5,6], thereby allowing compressive and tensile stresses during bending to be predicted. The elastic modulus and the Poisson ratio are inputs of the model and need to be measured for each sample, because they depend on the latex type, starch loading, and the paper fiber properties. One drawback of FEM is that it does not lead to particle scale insights of the mechanism of crack formation.

Some continuum type models have been explored by modeling groups of particles connected by polymeric bridges [7]. When the number of particles increases and the distance between particles is small, the numerical analysis of this nature becomes costly. While some insight into mechanical properties of porous composites has been obtained with a mesh-free continuum mechanics simulation [8], an understanding of micromechanical behavior of pigmented coating layers in various industrially relevant situations is lacking.

Discrete element methods (DEM) are based on the particle length scale and have the potential to reveal particle level mechanisms in the study of these systems. Toivakka and Bousfield proposed a simple model to predict the dynamic mechanical properties of a pigmented coating layer in tension and compared the simulation results to experimental data [9]. Discrete element methods have been used to study the compression of paper coatings during the calendering event [10]. Tensile and bending predictions have also been reported previously by Varney and Bousfield for two-dimensional (2D) models [11,12]. Most of these models are 2D in nature, except Azadi et al. [10], and as a consequence, comparisons between 2D and three-dimensional (3D) models have not been reported.

While most of the past 3D DEM work has involved the use of monodisperse spherical particles, some work has used other shapes and particle size distributions (PSDs).

Azadi and coworkers [10] used spherical particles similar in size and distribution to two ground calcium carbonates (GCCs, 60 w/w% < 2 µm and 90 w/w% < 2 µm) and a hypothetical pigment with a bimodal PSD [10]. In a second study, they used commercially available software to model spherical, needle-like, and platy particles [13]. The latter two shapes were modeled as a collection of spherical particles "attached" to each other. Two PSDs were modeled for each particle shape — a monodisperse and a polydisperse. Other investigators used multiple size distributions for 2D DEM work [14] and with the FEM [6,14]. The latter work included spherical as well as platy particles in its model.

The current work uses a particle level model to understand the tensile and bending behavior of a coating layer that contains mineral pigment, latex, and starch. Two different PSDs for the spherical pigments are evaluated, as well as bimodal and pseudo-full distributions. The results are compared with experimental data [15,16]. Latex and starch mixtures were used as a binder between GCC pigments in these experiments, and the mechanical properties of these binder mixtures are inputs into the model. The predictions of 3D forms of the model are compared along with the experimental values for two pigment volume concentrations (PVCs).

MODEL DESCRIPTION

When two pigments move relative to each other, as in the example of in-line tension shown in **Fig. 1**, a restoring force is calculated to pull them together based on the local strain of the polymer between them.

The force equation used here takes on the non-linear form of:

$$F = A(1-e^{-B\varepsilon})\pi R_b^2 \quad (1)$$

where F is the tensile force between particles, A and B are parameters that depend on the pure binder properties, ε is the local strain between particles, and R_b is the radius of the binder bridge between particles. The bridge radius and the spacing of the particles depends on the pigment volume fraction (*PVC*), which is defined as the ratio of total volume of pigments to the volume of pigments plus the volume of binder. The relationship between the *PVC* and the binder bridge radius was discussed by Varney and Bousfield [17]. In this work, the binder bridge radius was found to fit the equation below, when the *PVC* is above the critical value:

$$R_b = (3.1 - 3.1PVC)^{0.25} \quad (2)$$

Critical PVC (*CPVC*) is defined as the pigment concentration where the pigments are packed as close as possible and the binder is exactly the amount required to fill in the space between the pigments. Note that as *PVC* approaches its maximum value of 1.0, the binder bridge radius goes to zero, corresponding to a system that has no binder. Below the *CPVC*, the binder bridge radius is equal to the particle radius. As such, the particle separation would increase as the *PVC* decreases. This value represents a system that is full of binder everywhere. Above the *CPVC*, the shape of the binder bridge is assumed to be cylindrical. Because the model is concerned with small deformations, R_b should not change to a large extent during deformation and is assumed to be constant. More complicated models could take this situation into account in the future.

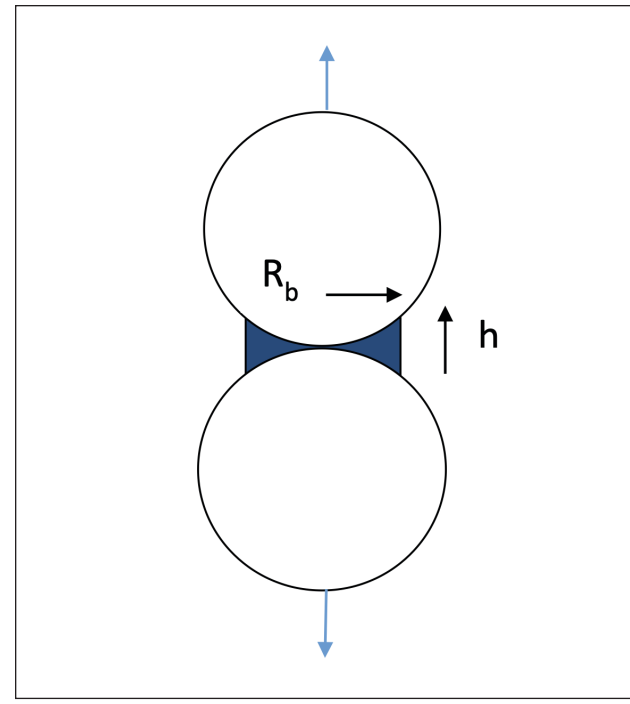

1. Idealized system of two spherical pigments connected together by a binder bridge. The binders of interest here are mixtures of starch and latex. R_b is the binder bridge radius and h is the length of the binder bridge.

When the predicted local strain between particles is larger than the strain-to-failure (*STF*) of the actual binder, the binder is assumed to fail cohesively, and the interparticle force is set to zero. The non-linear form for the force, Eq. 1, is selected because it resembles the behavior of the tensile tests of the binder films as reported by others [18,19]. While the model can also account for adhesive failure at pigment surfaces with a critical strain or stress criteria, the current work assumes that cohesive failure in the binder is the dominant mechanism.

The mechanical properties of binder films consisting of starch and latex mixtures are reported by Zhu et al. and Najafi et al. [15,16]. The experimentally measured maximum *STF* in tension is the parameter A in Eq. 1. The elastic modulus (E) divided by A is the parameter B in Eq. (1), because the initial slope of this equation is the product of A and B. **Table I** summarizes the mechanical properties

Investigator	Weight Fraction Latex, Parts	*A*, MPa	*B*	*E*, MPa	*STF*, %
Najafi et al.	100	1.5	2	3	200
Najafi et al.	80	4.9	15	73.5	80
Najafi et al.	60	4.8	35	168	22
Najafi et al.	40	11.0	60	660	5
Zhu et al.	100	3.75	3.2	12	355
Zhu et al.	77	9.4	24	221	200
Zhu et al.	58	15.5	29	448	41
Zhu et al.	38	32.0	36	1156	13

I. Mechanical properties of particle free films composed of mixtures of starch and latex and the values of A and B in the model.

of the films produced from mixtures of latex and starch and the corresponding parameters *A* and *B*. As is well known, as starch is added to these systems, the elastic modulus of the binder increases, but the *STF* decreases.

If particles move closer to each other compared to the initial gap (compression), a repulsive force is applied to keep the particles from overlapping. This repulsive force is linear and depends on the compressive strain as:

$$F = C\varepsilon \tag{3}$$

where C is some constant, and the strain is the current gap between particles divided by the initial gap.

Another parameter included in the model is the distance between two particles within which they can still be considered neighbors and, thus, are assumed to have a connection (R_n). While at the *CPVC*, every particle is close to several others, and it is not clear at what distance particles should be considered connected. In **Fig. 2**, if the gap between the particle of interest and the other particles is less than one radius, the particles will be considered neighbors and will, therefore, be connected. If they are further away, then no connection is assumed.

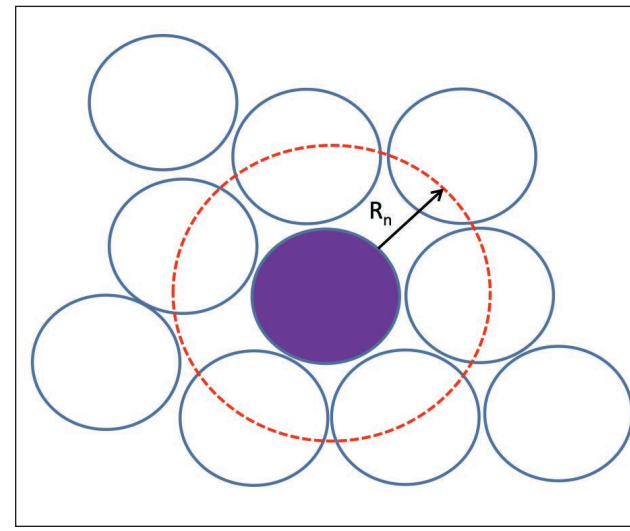

2. Near neighbor criteria with R_n = 1.0. Particles closer than the criteria are assumed to be connected. As R_n increases, more particles are connected together.

Particle size distributions

The main difference between this work and the previous studies [20] is the move beyond a monodisperse packing of spherical particles to two other distributions of the same particle shape. The first one is bimodal distributions of large and small spheres. The amounts, or levels, of each size were based on the work of [21]. This paper showed that the void fraction of bimodal mixtures was a function of the size ratio $u = d_L/d_S$ (where d_L is the diameter of the large particle and d_S is the diameter of the small particle) and of the volume fraction of the large particle. Here, to cover a range of void fractions, three size ratios (5, 3.33, and 2.5) were used for each of three volume fractions of the large particles (0.80, 0.65, and 0.50).

In addition to these nine bimodal distributions, two distributions that represented a coarse GCC (60 w/w% < 2 µm) and a narrow particle size GCC (93 w/w% < 2 µm) were also evaluated; these should be similar to the GCC types used [15,16]. To generate data for the particle packing routine, PSD data for two commercially available GCCs from Omya Inc. (Oftringen, Switzerland) was obtained and discretized to include approximately one decade of particle sizes.

The particle packing routines as described in the following paragraphs were used to generate the (x, y, z) coordinates for the nine bimodal cases, the two GCCs, and a monodisperse case. As with all prior simulations, the particle coordinates were inputs to the model, along with the mechanical properties of the pure binder films.

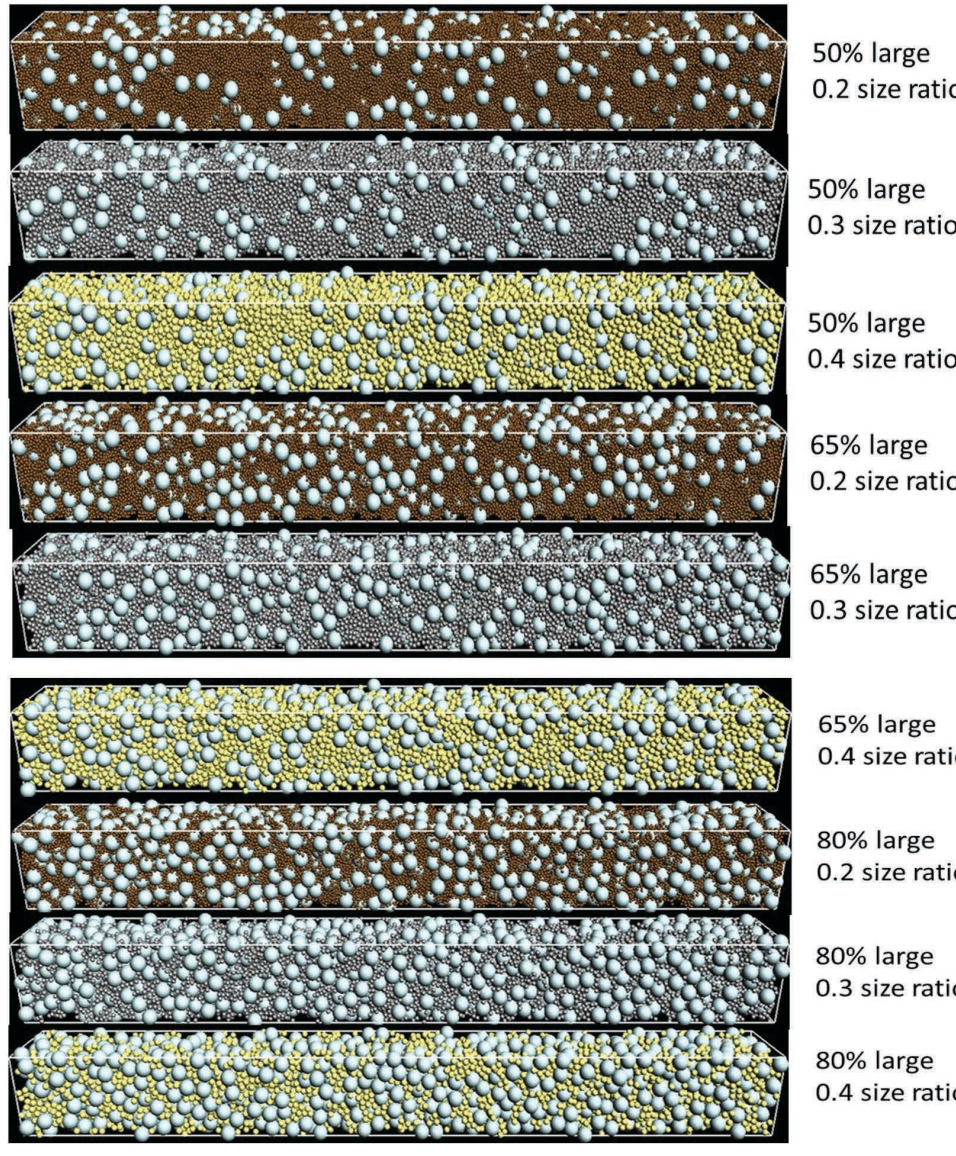

3. Examples of bimodal packing of spheres in a three-dimensional geometry for various size ratios and volume concentrations of large particles.

Initial particle positions in the 3D packings were generated with a voxel-based digital packing tool detailed in [22]. Subsequently, the porosity of the packings was adjusted to a desired level by using a particle packing approach mimicking Brownian motion. In this case, an energy function calculated from the particle positions and interparticle distances was minimized towards the desired porosity utilizing a simulated annealing algorithm [23]. The simulation box size for all the cases was 10 μm^3 x 10 μm^3 x 100 μm^3, and periodic boundary conditions were applied in all three directions.

The simulated packings of the nine bimodal distributions and the two full distributions (representing the two GCCs) are shown in the **Figs. 3–5**. The bimodal figures show the changing volume ratio of small to large particles, as well the change in the small particle size. The total number of particles in a packing varied from 6000 to 115000, depending on the PSD used. **Figure 6** shows how the packing density depends on the fraction of the large particles and the size ratio. The maximum packing is obtained around 65% large particles, which agrees with previous studies packing bimodal spheres [24,25]. A smaller size ratio also leads to higher packing density due to the small particles being able to more efficiently fill in the spacing between the large particles.

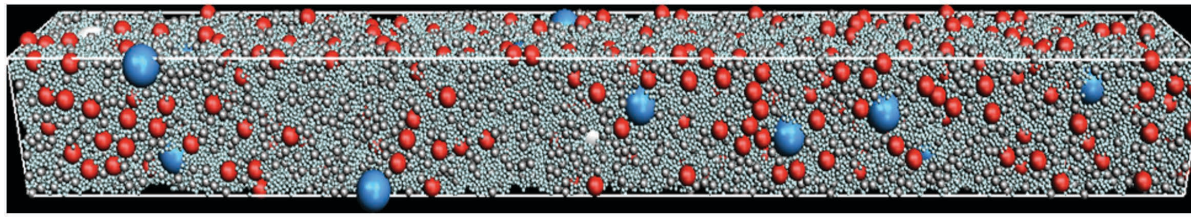

4. Representation of full distribution of spherical particles approximating a narrow particle size ground calcium carbonate (GCC; 93 w/w% < 2.0 µm; particle size range 0.35–4.0 µm; simulated with 5 particle size bins; packing density 66.2%).

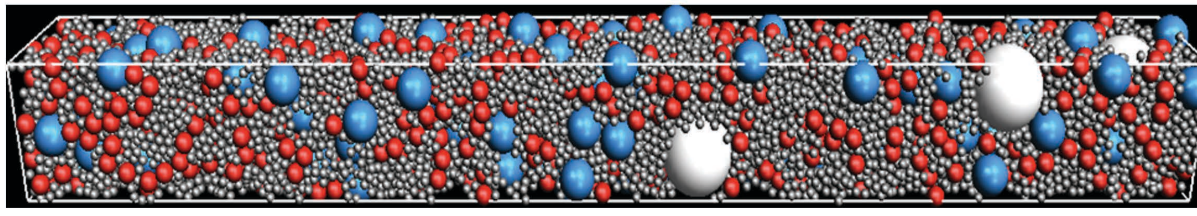

5. Representation of full distribution of spherical particles approximating a broad particle size GCC (60 w/w% < 2.0 µm; particle size range 0.75–6.0 µm; simulated with 4 particle size bins; packing density 65.7%).

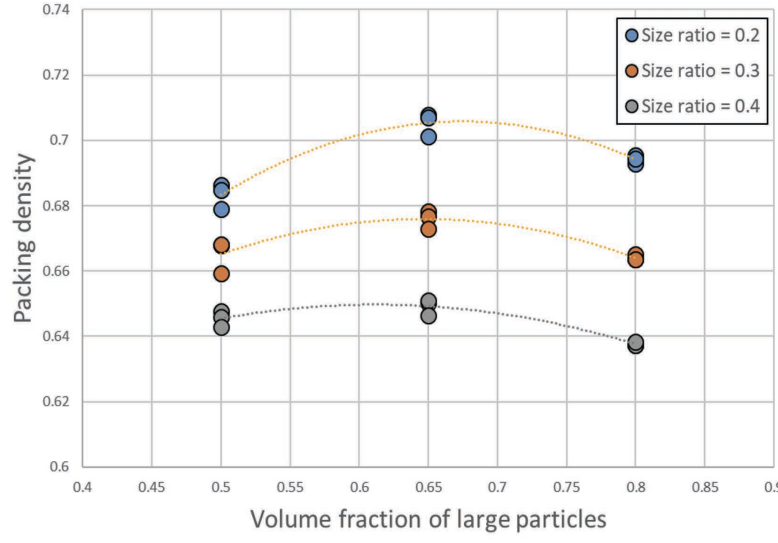

6. Packing density as a function of large particle volume fraction for different size ratios used in the simulated particle packings.

Modeling of in-line tension and of three-point bending

To simulate an in-line tensile event, particles in the grip region on the right of **Fig. 7** are set to a velocity of one dimensionless unit towards the right. Particles in the left grip region are assigned to no velocity. This scenario causes the particles on the right to pull on other particles in the middle of the structure and transmit forces throughout the structure. The results presented here are for slow motions relative to the inertia of the particles. Therefore, the forces are near equilibrium during the deformation event, and the rate of deformation is not important.

To stabilize the simulation when a crack occurs, it was found helpful to add a small damping factor where a particle moving at some velocity will experience a force in the opposite direction according to:

$$F = -DV \tag{4}$$

where D is a damping factor, and V is the velocity vector.

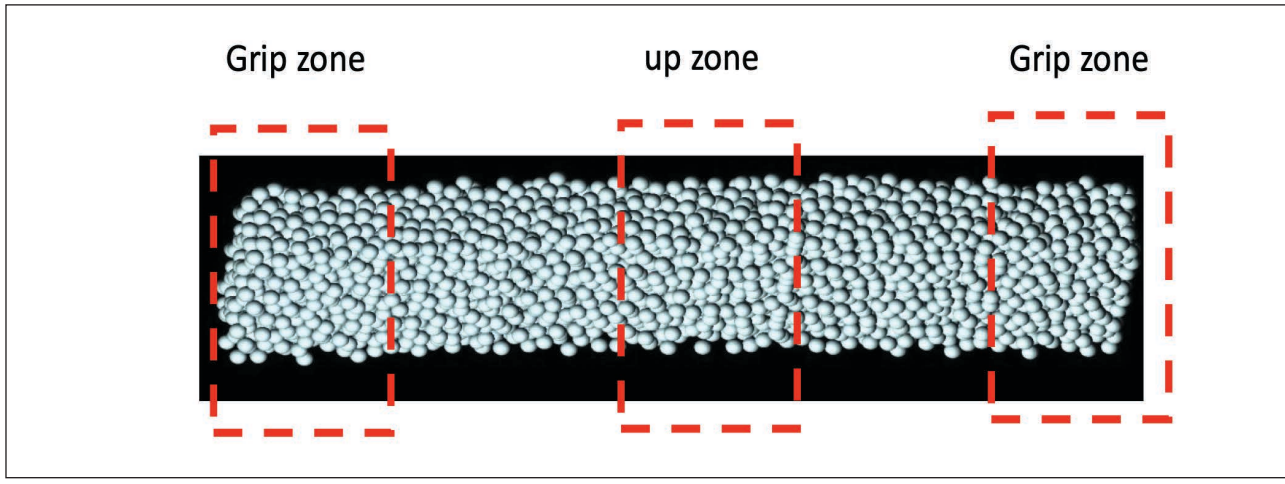

7. A 3D situation for monodisperse spheres packed in a 10 µm³ x 10 µm³ x 100 µm³ cell. Particles are packed to a pigment volume concentration (PVC) of 64%. Left and right boxes are where spheres are held still and moved to the right, respectively, for tension. The center box shows where spheres are moved upward for bending simulations.

The value of the damping factor should be small in order to not influence the predictions of the modulus or of the ultimate stress.

To simulate bending tests, particles in the "push up" zone are assigned an upward velocity depicted in Fig. 7. Spheres on the two sides (the grip zones) of the simulation are not allowed to move in the vertical direction, but they are allowed to slide in the horizontal direction or deflect downward. The sizes of the holding (grip) zones and of the push up zone have minimal influence on the results, as long as the distance from the zones is large compared to the zones themselves.

In both cases, as some particles are forced to move from their equilibrium position, a vector force on neighboring particles is calculated using either Eq. 1 or the compression Eq. 3. The net force on every particle is calculated based on its position and the position of all of the neighbors. This net force is used to update particle velocities and positions with a numerical integration using a predictor-corrector method. In the results presented in this paper, the motion is slow and the inertia terms are small; time or rates do not influence the results, but these effects are straightforward to include in the future. The time integrations can be expressed as:

$$a = dV / dt = F / x_m$$
$$dP / dt = V \quad (5)$$

where a is the acceleration vector, V is the velocity vector, F is the force vector, x_m is a parameter that represents the mass of the particle, and P is position. Equation 5 is a vector equation, because it has components in each dimension.

The sum of the forces on the particles that move relate to the force a mechanical tester would record; these forces balance the sum of the forces on the particles that are not allowed to move. In tension, the stress is the sum of the forces on the grip particles divided by the cross-sectional area. The flexural stress and strain can be calculated as:

$$\sigma_f = \frac{3PL}{2bd^2} \quad (6)$$

$$\varepsilon_f = \frac{6Dd}{L^2} \quad (7)$$

where P is the sum of the forces on the grip particles (or the load force), L is the distance between grips, D is the displacement of the upward moving particles at the center of the sample, b is the width of the sample, and d is the thickness of the sample. The goal is to predict the bending behavior and the crack propagation of these systems.

The deformation and local forces are shown in **Fig. 8** for a typical three-point bending case. In the region that is forced upward, a tensile force is generated. Also, near the region where particles are only allowed to slip in the horizontal direction, a tensile force is generated between particles. When particles separate more than the binder strain-to-failure, the force is turned off, and a crack is formed and propagated through the structure.

RESULTS AND DISCUSSION

Tensile properties

The predictions of the models are compared to the in-line tensile experimental data of Zhu et al. [15] in **Fig. 9** for the *PVC* near the critical value of 63% by volume of pigment and for the 77% latex/23% starch binder package (77L/23S). The model was run using the nine different bimodal distributions, the uniform spheres, and the pseudo-Hydrocarb 60 (H60) distribution that should represent the GCC used in the experiments. The values for the input parameters *A*

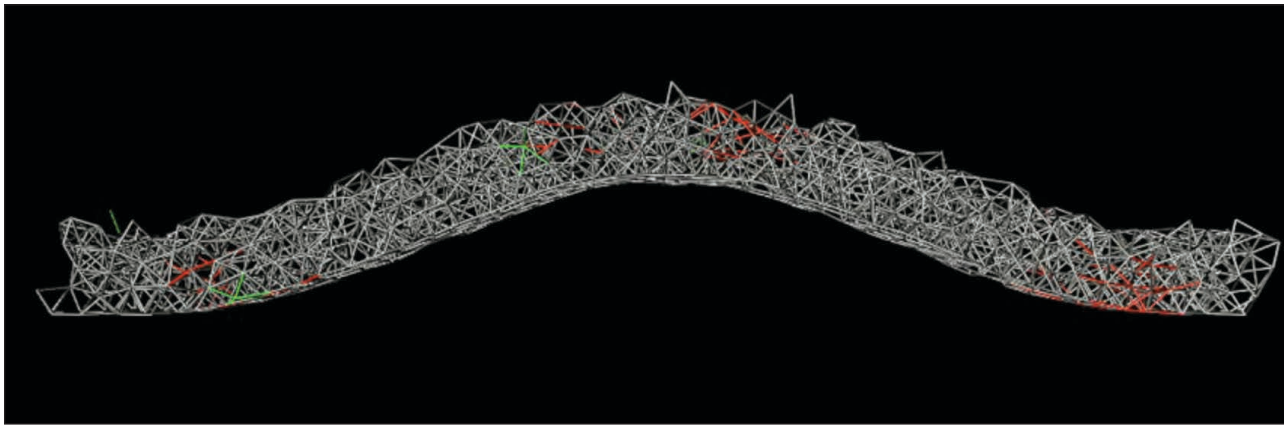

8. Bending deformation in 3D mode showing the connections between particles for a typical case for monodisperse spheres. Red color indicates tension between pigments.

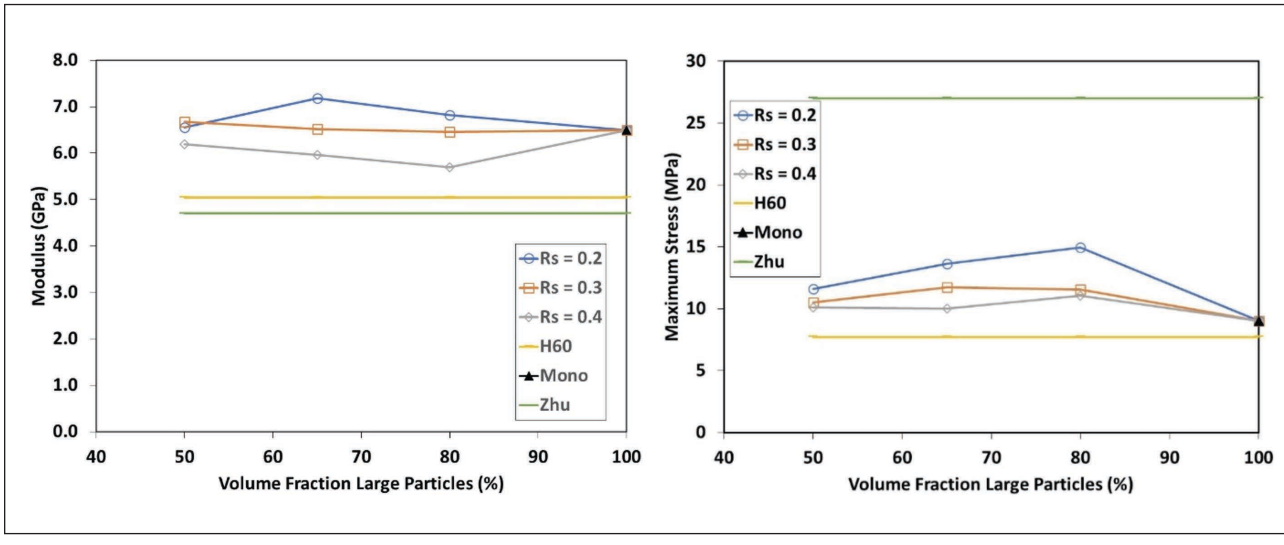

9. Elastic modulus (left) and maximum stress (right) of coating layer for in-line tension at PVC = 63% and with the 77L/23S binder system (Rs = small particle radius).

and *B* were taken from the 77L/23S pure binder data. Other important model parameters were values of R_n = 1.0 and R_b = 1.0. The modulus is plotted vs. the volume fraction of larger particles with three lines representing the small particle radii (0.2, 0.3, and 0.4). In addition, data points for the Zhu data and for the pseudo-H60 are shown as horizontal lines across the range of *x* values. Lastly, the mono-disperse case is shown as a single data point at the 100% large particle point on the *x* axis.

The elastic modulus predictions for the pseudo-H60 results are 6% higher than the value from Zhu's experiments of 4.7 GPa. The bimodal distribution with a small particle radius (R_s) of 0.4 comes the closest to matching this value, but it still exceeds the Zhu data like the rest of the bimodal simulations. One trend to note is the increase in modulus as the radius of the small particle decreases, which occurs for each volume fraction of large particles. The reason for this trend is that the number of particles and, hence, the "tightness" or density of the packing increases as the small particle radii decrease. With more particles filling the voids between the larger ones, fewer and smaller voids are resulting, which leads to more connections. As a consequence, the strength will increase with a denser packing. This agrees with the Rättö et al. [26] explanation of their results when comparing the improved strength data for a broad particle size GCC vs. a narrow distribution GCC.

The pseudo-H60 data point is lower than the rest, which might imply a fairly open packing that is due to a large average particle size (about 1.4 µm). A contributing factor can also be the exclusion of very small particles (< 0.75 µm) in the packing due to computational resource limitations caused by them.

In contrast to the modulus, the maximum stress predictions given in Fig. 9 show the model results to be significantly below the experimental value of 27.0 MPa. The monodisperse and pseudo-H60 data points are below all three bimodal lines, which also all appear to trend upwards. In addition, the data from the experiments and for

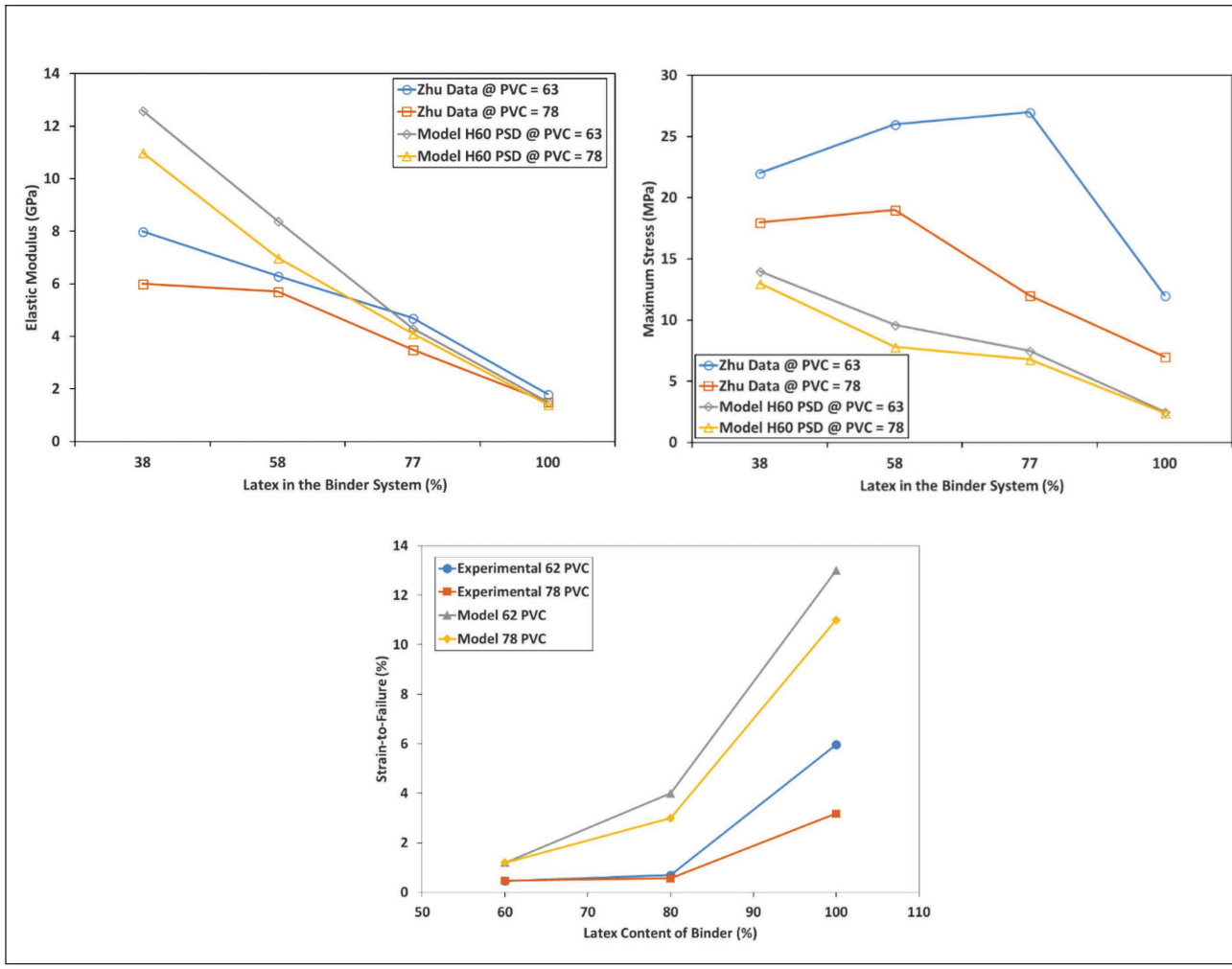

10. Elastic modulus (left), maximum stress (right), and strain-to-failure (bottom) comparison between data and the model at two PVCs for in-line tension for different starch/latex content.

the pseudo-H60 case are quite different. The reasons for the poor performance of the model to predict the maximum stress are not clear, but if the *STF* of the latex-starch films is different than the behavior of the material in a coating layer, this could explain the difference. Also, another possible reason is that the packing routine of the pigments does not account for the latex binder. Particles may be packing in a slightly different configuration that could explain the differences. The *STF* simulation results are also low compared to the data. As Zhu et al. [15] discuss, the starch tends to behave as a pigment in the experiments. The same trends followed in both cases, with the pseudo-H60 being the lowest for the *STF* results as well.

Figure 10 shows the comparison of the experimental tension data with the model at two PVCs and four different latex/starch ratios in each case. While the experimental work was done at several pigment volume concentrations, the values of 63 (which is the *CPVC*) and 78 were chosen. The modulus plot in Fig. 10 shows the model to approximate the experimental data quite well, especially at higher latex content in the binder system. At the lowest level of latex (38%), the model overpredicts the modulus. In addition, the values at a *PVC* of 78 are lower than the corresponding values at a *PVC* of 63. These results make sense, as there is less binder in the matrix relative to the amount of pigment above the *CPVC*, which should lead to a drop in strength. And, as has been seen in the past, the modulus decreased as the level of latex in the binder system increased or as the amount of starch was reduced.

The maximum stress plots in Fig. 10 shows some of the same general trends, except the model underpredicts the magnitude of this property by around 50%. The higher 78 *PVC* results for both the model and the experimental work were lower than the 63 *PVC* conditions, and the overall curves decreased directly with the starch level.

The *STF* results reveal the same trends as have been seen before. The model and the experimental data are in good agreement at low levels of latex in the binder package but start to diverge as the latex percentage increases, especially when the binder is all latex. The model underpredicts the Zhu et al. data as well.

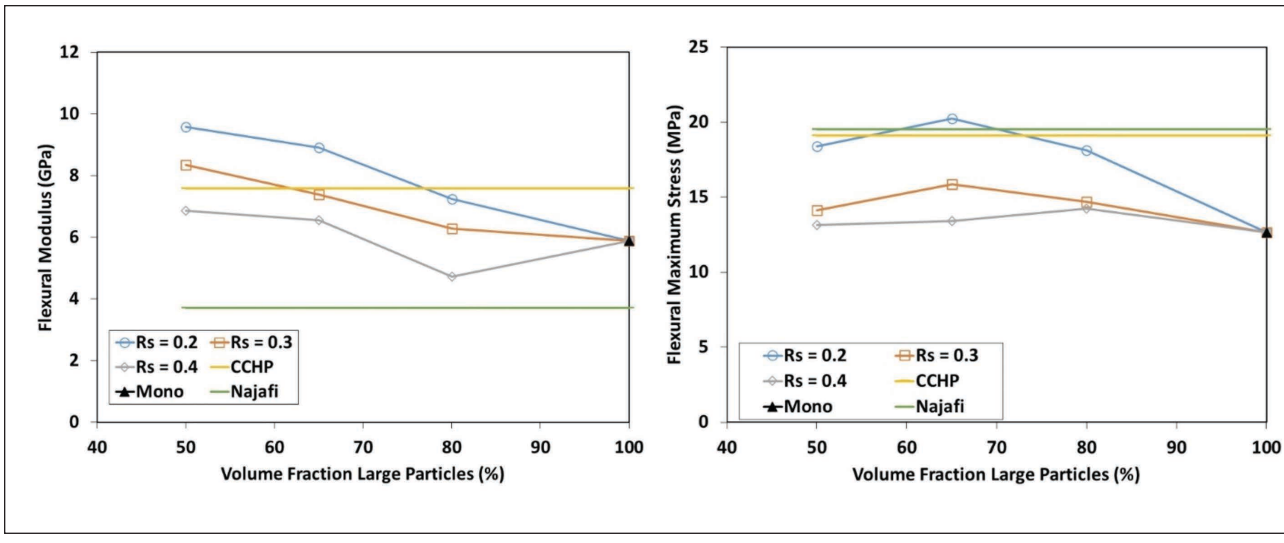

11. Predicted and measured flexural modulus (left) and maximum stress (right) for the coating layer near PVC of 63% for binder components of various levels of starch and latex (three-point bending).

Three-point bending

The predictions of the model are compared to the three-point experimental data of Najafi et al. [16] in **Fig. 11** for the *PVC* near the critical value of around 63% by volume of pigment and for the 80% latex/20% starch binder package (80L/20S). The same particle size distributions were run in this comparison as was done with Zhu et al., but the pseudo-H60 was replaced with a distribution that approximated Covercarb HP. In addition, the model input parameters A and B were taken from the 80L/20S pure binder data and, as before, the values for R_n and for R_b were 1.0 in each case.

The flexural modulus predictions in Fig. 11 overpredict the Najafi modulus value of 3.7 GPa. The bimodal distribution with 80% large particles by volume and a small particle radius of 0.4 comes the closest to experimental results. This overprediction could be related to the difference in the length scales of the simulation compared to the experiments, because in the model, only a small length is bent but the experiments deform a strip of coating.

The prediction of the maximum flexural stress is in excellent agreement with the data when using the pseudo narrow particle size distribution. The bimodal distribution with a small particle radius of 0.2 is also a good match to these two horizontal data lines. The monodisperse data point is the result furthest from the experimental data line of Najafi et al. [16], which could be a function of the impact of packing on strength.

In the three-point bending simulation, the amount of strain, as defined in Eq. 7, when a crack first forms is predicted and sets the *STF* of the system. The *STF* predictions are given in **Fig. 12** and show good agreement between the data and the pseudo narrow size distribution prediction. The three bimodal lines also are reasonably close to the experimental results. As with the maximum stress, the monodisperse data point is significantly different from the other data points, whether they are from the experiments or from the model.

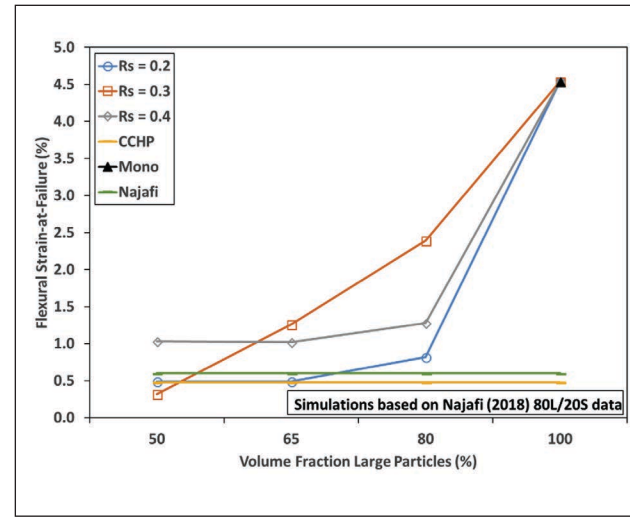

12. Predicted and measured strain-to-failure for coating layers near PVC of 63% for various levels of latex and starch in the binder composition.

As with the in-line tension results, the three-point bending predictions showed some gains relative to the experimental data when switching from uniform spheres to either bimodal or full distributions of spheres. The results were also not consistent in terms of the trends, but the general observation was that some improvements were obtained.

Figure 13 shows the comparison of the model for the two different *PVC*s (63 and 78) of Najafi et al. [16] as the latex/starch content changes in the coating. As with the other comparisons, the binder bridge radius, for a *PVC* of 78%, is 90% of the particle radius of the particle of interest based on Eq. 2. This value reduces the modulus predictions and the maximum stress predictions around that factor, but the *STF* remains quite similar.

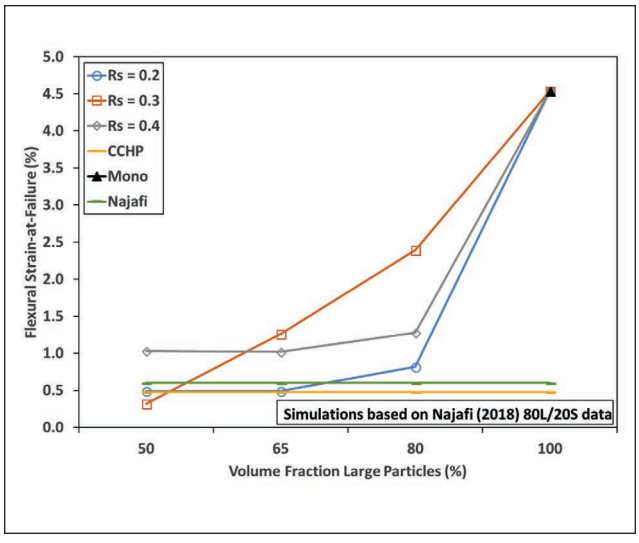

13. Flexural modulus predictions (left) and maximum stress (right) compared to experimental results at two PVCs (three-point bending) for different latex concentrations in the binder system.

The flexural modulus results in Fig. 13 overpredict the experimental data for both *PVC*s, except for the latex only results. These results are in contrast to the in-line tension comparison with Zhu's data. Regardless, both sets of data show the same trends in that the higher *PVC* condition has a lower modulus value, and the lines trend downwards with increasing latex percentage in the binder system.

The maximum stress predictions are reasonably close to the data at 62 *PVC*. For some reason, the 78 *PVC* experimental data is significantly different from the other lines. This *PVC* is a brittle coating, and mounting the sample in the mechanical tester may lead to some loss of strength. The *STF* predictions are in good agreement with the experimental data.

Packing density influence on mechanical properties

Figure 14 shows the modulus predictions for both in-line tension and for three-point bending as a function of packing density. The data for both cases show an upward trend in modulus as the packing density increases. As the particles are packed more tightly, the gap between particles on average decreases, which causes the initial strain between pigments to increase for the same amount of sample strain, resulting in an increase in the modulus. The maximum stress reported in Fig. 14 follows the same trend. The two curves show an increase in values as the packing density increases. The same reasoning for the trend in modulus explains this result as well. Similar trends are seen in the behavior of the *STF* predictions based on packing density.

CONCLUSION

A discrete element method model was developed to predict the mechanical properties of pigmented coating layers. The model input parameters are the mechanical properties of the binder, the pigment volume concentration, and the particle size distribution. The model gives reasonable predictions for both tensile and flexural tests and does predict most of the correct trends. For in-line tension, the model predicts the modulus, but underpredicts the maximum stress and strain-to-failure. For bending, the model predicts well the maximum stress. In general, the move from uniform spheres to bimodal and full particle size distributions did provide some improvement in predictions. The packing density of the pigments is found to be an important parameter that influences the mechanical properties of the coating layer. **TJ**

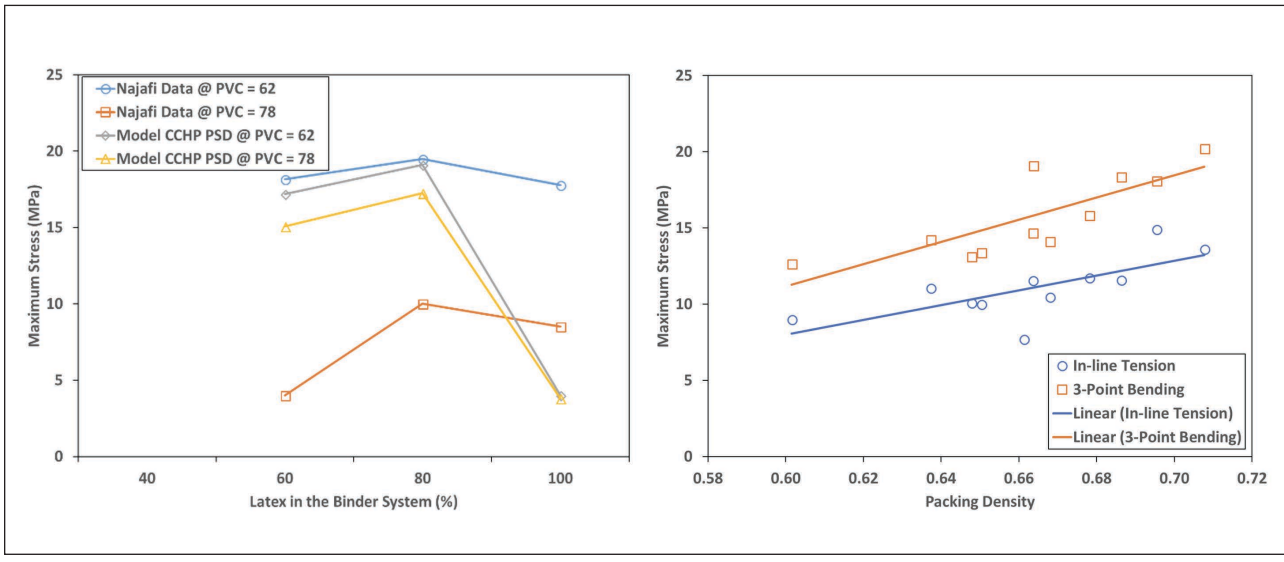

14. Modulus predictions (left) and maximum stress (right) as a function of packing density for in-line tension and three-point bending.

ACKNOWLEDGEMENTS

We would like to thank the sponsors of the University of Maine Paper Surface Science Program for their discussions and support.

LITERATURE CITED

1. Sim, K., Youn, H.J., Oh, K.D., et al., *Nord. Pulp Pap. Res. J.* 27(2) 445(2012). https://doi.org/10.3183/npprj-2012-27-02-p445-450.
2. Barbier, C., Rättö, P., and Hornatowska, J., "Coating models for an analysis of cracking behavior between folded paper and creased board," *TAPPI Adv. Coat. Fundam. Symp., 12th*, TAPPI Press, Peachtree Corners, GA, USA, 2012.
3. Rättö, P. and Hornatowska, J., *Nord. Pulp Pap. Res. J.* 25(4): 495(2010). https://doi.org/10.3183/npprj-2010-25-04-p495-501.
4. Oh, K., Sim, K., Jung, Y.B., et al., *Nord. Pulp Pap. Res. J.* 30(2): 360(2015). https://doi.org/10.3183/NPPRJ-2015-30-02-p360-367.
5. Barbier, C., Larsson, P.-L., and Ostlund, S., *Compos. Struct.* 67(4): 383(2005). https://doi.org/10.1016/j.compstruct.2004.01.024.
6. Alam, P., Toivakka, M., Carlsson, R., et al., *J. Compos. Mater.* 43(11): 1265(2009). https://doi.org/10.1177/0021998308104227.
7. Rättö, P., *J. Pulp Pap. Sci.* 30(12): 335(2004).
8. Toivakka, M., Alam, P., Touaiti, F., et al., *TAPPI J.* 14(6): 373(2015). https://doi.org/10.32964/TJ14.6.373.
9. Toivakka, M. and Bousfield, D., "Modeling of coating layer mechanical properties," *TAPPI Adv. Coat. Fundam. Symp.*, TAPPI Press, Atlanta, 2001.
10. Azadi, P., Farnood, R., and Yan, N., *Comput. Mater. Sci.* 42(1): 50(2008). https://doi.org/10.1016/j.commatsci.2007.06.007.
11. Varney, D. and Bousfield, D., "Discrete element method to predict coating failure mechanisms," *PaperCon*, TAPPI Press, Peachtree Corners, GA, USA, 2017.
12. Varney, D. and Bousfield, D., "Discrete element method to model cracking for two layer systems," *PaperCon*, TAPPI Press, Peachtree Corners, GA, USA, 2018.

ABOUT THIS PAPER

Cite this article as:
Varney, D., Toivakka, M., and Bousfield, D.W., *TAPPI J.* 22(7): 491(2023). https://doi.org/10.32964/TJ22.7.491

DOI: https://doi.org/10.32964/TJ22.7.491

ISSN: 0734-1415

Publisher: TAPPI Press

About this journal

13. Azadi, P., Farnood, R., and Yan, N., *Comput. Chem. Eng.* 32(12): 3084(2008). https://doi.org/10.1016/j.compchemeng.2008.05.001.
14. Alam, P., Toivakka, M., Lazarus, E., et al., "On the mechanisms of wet and dry strength of paper coatings–Part 2–Modeling and simulation," *PaperCon*, TAPPI Press, Atlanta, 2012.
15. Zhu, Z., Salminen, P., Chen, G., et al., "Mechanical properties of pigment coating composites containing starch," *TAPPI Adv. Coat. Fundam. Symp., 13th*, TAPPI Press, Peachtree Corners, GA, USA, 2014.
16. Najafi, S.M.H., Tajvidi, M., and Bousfield, D.W., *Prog. Org. Coat.* 123: 138(2018). https://doi.org/10.1016/j.porgcoat.2018.07.009.
17. Varney, D. and Bousfield, D., "Improved discrete element method model to predict coating layer mechanical properties," *PaperCon*, TAPPI Press, Peachtree Corners, GA, USA, 2016.
18. Prall, K.M., Shaler, S.M., and LePoutre, P.F., *Nord. Pulp Pap. Res. J.* 15(5): 564(2000). https://doi.org/10.3183/npprj-2000-15-05-p564-571.
19. Raman, K., Bousfield, D.W., and Shaler, S.M., "Analyzing the effect of binder content on the mechanical properties of paper coatings," *TAPPI Coating–Papermakers Conf.*, TAPPI Press, Atlanta, 1998.

ABOUT THE AUTHORS

We studied this topic at the suggestion of an industry group, and we compared results from past experiments with cracking with our model. The most difficult aspect of this research was that bending simulations take time. We addressed this by running the laptop while traveling.

From this research, we discovered the influence of packing density. Of particular interest was the slight improvement in model predictions compared to uniform spheres.

With this study, mills can better understand how coating formulation influences cracking. Our next step is to study cracking in barrier coatings.

Varney is principal consultant at Marble Hill Consulting in Proctor, VT, USA. Toivakka is professor, Paper Coating and Converting, at the Laboratory of Natural Materials Technology, Åbo Akademi University, in Turku, Finland. Bousfield is Calder professor in the Paper Surface Science Program, Department of Chemical and Biomedical Engineering, at the University of Maine in Orono, ME, USA. Email Bousfield at bousfld@maine.edu.

Varney

Toivakka

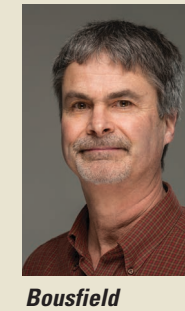

Bousfield

20. Varney, D., Bousfield, D., and Toivakka, M., "Discrete element method to model tension and bending for single layer 3-dimension systems," *PaperCon*, TAPPI Press, Peachtree Corners, GA, USA, 2019.
21. Brouwers, H.J.H., *Physical Rev. E* 84: 042301(2011). https://doi.org/10.1103/PhysRevE.84.042301.
22. Byholm, T., Toivakka, M., and Westerholm, J., *Power Technol.* 196(2): 139(2009). https://doi.org/10.1016/j.powtec.2009.07.013.
23. Corana, A., Marchesi, M., Martini, C., et al., *ACM Trans. Math. Software* 13(3): 262(1987). https://doi.org/10.1145/29380.29864.
24. Lam, D.C.C. and Nakagawa, M., "Effect of particle size distribution shape in bimodal packing," in *Advanced Materials '93* (N. Mizutani, K. Akashi, T. Kimura, et al., Eds.), Elsevier, Amsterdam, 1994. https://doi.org/10.1016/B978-0-444-81991-8.50032-7.
25. Averardi, A., Cola, C., Zeltmann, S.E., et al., *Mater. Today Commun.* 24: 100964(2020). https://doi.org/10.1016/j.mtcomm.2020.100964.
26. Rättö, P., Hornatowska, J., and Barbier, C., *Nord. Pulp Pap. Res. J.* 27(4): 714(2012). https://doi.org/10.3183/npprj-2012-27-04-p714-720.